2016

Distinction in corrosion resistance of selective laser melted Ti-6Al-4V alloy on different planes

Nianwei Dai
Shanghai University of Engineering Science

Laichang Zhang
Edith Cowan University

Junxi Zhang
Shanghai University of Engineering Science

Xin Zhang
Shanghai University of Engineering Science

Qingzhao Ni
Shanghai University of Engineering Science

See next page for additional authors

10.1016/j.corsci.2016.06.009
This is an Author's Accepted Manuscript of:
Dai, N., Zhang, L., Zhang, J., Zhang, X., Qingzhao, N., Chen, Y., ...Yang, C. (2016). Distinction in corrosion resistance of selective laser melted Ti-6Al-4V alloy on different planes. Corrosion Science, 111, 703-710.
https://doi.org/10.1016/j.corsci.2016.06.009

2016

Distinction in corrosion resistance of selective laser melted Ti-6Al-4V alloy on different planes

Nianwei Dai
Shanghai University of Engineering Science

Laichang Zhang
Edith Cowan University, l.zhang@ecu.edu.au

Junxi Zhang
Shanghai University of Engineering Science

Xin Zhang
Shanghai University of Engineering Science

Qingzhao Ni
Shanghai University of Engineering Science

See next page for additional authors

10.1016/j.corsci.2016.06.009
Originally published as: Dai, N., Zhang, L., Zhang, J., Zhang, X., Qingzhao, N., Chen, Y., ...Yang, C. (2016). Distinction in corrosion resistance of selective laser melted Ti-6Al-4V alloy on different planes. *Corrosion Science*, 111, 703-710. Original article available here

Authors
Nianwei Dai, Laichang Zhang, Junxi Zhang, Xin Zhang, Qingzhao Ni, and Yang Chen

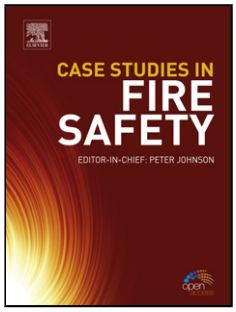

Title: Distinction in Corrosion Resistance of Selective Laser Melted Ti-6Al-4 V Alloy on Different Planes

Author: Nianwei Dai Lai-Chang Zhang Junxi Zhang Xin Zhang Qingzhao Ni Yang Chen Maoliang Wu Chao Yang

PII: S0010-938X(16)30279-7
DOI: http://dx.doi.org/doi:10.1016/j.corsci.2016.06.009
Reference: CS 6817

To appear in:

Received date: 28-3-2016
Revised date: 7-6-2016
Accepted date: 8-6-2016

Please cite this article as: Nianwei Dai, Lai-Chang Zhang, Junxi Zhang, Xin Zhang, Qingzhao Ni, Yang Chen, Maoliang Wu, Chao Yang, Distinction in Corrosion Resistance of Selective Laser Melted Ti-6Al-4V Alloy on Different Planes, Corrosion Science http://dx.doi.org/10.1016/j.corsci.2016.06.009

Distinction in Corrosion Resistance of Selective Laser Melted Ti-6Al-4V Alloy on Different Planes

Nianwei Dai [a], Lai-Chang Zhang [b,*], Junxi Zhang [a,*], Xin Zhang [a], Qingzhao Ni [a], Yang Chen [a], Maoliang Wu [a], Chao Yang [c]

[a] *Shanghai Key Laboratory of Materials Protection and Advanced Materials in Electric Power, Shanghai University of Electric Power, Shanghai 200090, PR China;*

[b]*School of Engineering, Edith Cowan University, 270 Joondalup Drive, Joondalup, Perth, WA 6027, Australia;*

[c]*National Engineering Research Center of Near-net-shape Forming for Metallic Materials, South China University of Technology, Guangzhou, 510640, China*

*Corresponding author. E-mail addresses: l.zhang@ecu.edu.au, lczhangimr@gmail.com (L.C. Zhang); zhangjunxi@shiep.edu.cn (J. Zhang).

Graphical abstract:

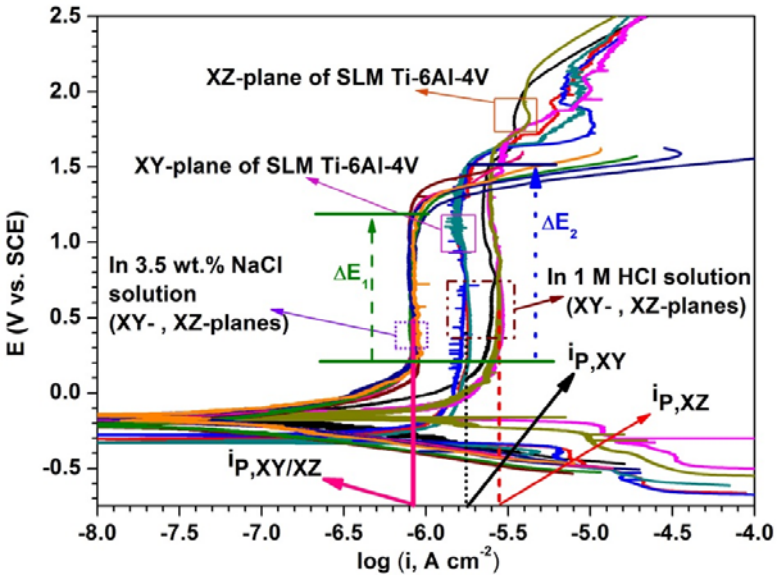

The SLM-produced Ti-6Al-4V alloy exhibits a higher corrosion rate in 1 M HCl solution than that in 3.5 wt.% NaCl solution and XZ-plane of the SLM-produced Ti-6Al-4V alloy gives rise to the inferior corrosion resistance compared with its XY-plane.

Highlights:

- Corrosion resistance of selective laser melted Ti-6Al-4V was investigated.
- XY-plane of Selective laser melted alloy shows a better corrosion resistance.
- More α' and less β-Ti weaken the corrosion resistance of XZ-plane.

Abstract: Electrochemical measurements and microstructural analysis were performed to study the corrosion resistance of different planes of Ti-6Al-4V alloy manufactured by selective laser melting (SLM). The electrochemical results suggest that its XY-plane possesses a better corrosion resistance compared to XZ-plane in 1 M HCl solution, in spite of slight difference in 3.5 wt.% NaCl solution, suggesting that the different planes exhibit more pronounced distinction in corrosion resistance in harsher solution system. The inferior corrosion resistance of XZ-plane is attributed to the presence of more α′ martensite and less β-Ti phase in microstructure for XZ-plane than for XY-plane of the SLM-produced alloys.

Keywords: A. Titanium; B. X-ray diffraction; B. EIS; B. SEM; C. Passivity

1. Introduction

Titanium (Ti) and its alloys have been increasingly used in many applications due to its excellent properties such as high strength, appropriate mechanical properties, high biocompatibility, and very good corrosion resistance [1-9]. Among them, Ti-6Al-4V is the most frequently utilized for biomedical, pipeline, marine and military applications [10-13]. Traditionally processed Ti-6Al-4V displays a duplex microstructure which is a mixture of α phase (hcp) and β phase (bcc) [3, 10], and its properties can be tuned by tailoring its microstructure through different heat treatment conditions. There have been many studies focusing on the corrosion behaviour of Ti-6Al-4V in various solution systems [14-17]; all these studies shed light on the corrosion behaviour of Ti-6Al-4V alloy and provided constructive suggestions on improving its corrosion resistance against service environments. At the same time, some conventional technologies such as laser treatment [11, 18], powder metallurgy [19, 20], space holder technology [21], halide treatment [22], surface coatings [23-26], plasma sintering [27], and foaming [28] were employed to improve the properties of Ti-6Al-4V alloy for the different application conditions. Razavi et al. [11] improved the corrosion behaviour of Ti-6Al-4V by means of laser gas nitriding. Pohrelyuk et al. [29] enhanced the corrosion resistance Ti-6Al-4V alloy via constructing a nitride coating on its surface. It is believed that the formation of dense and protective films improves considerably the corrosion resistance of Ti-based alloys. However, the emerging problem is that the high reactivity of Ti with oxygen and high melting point give rise to many challenges to these conventional technologies. Therefore, the improved properties through these traditional treatments limit the applications in different environments where the Ti-6Al-4V alloy is used.

Selective laser melting (SLM) is well known as one of important emerging additive manufacturing techniques. Considering the layer-wise additive nature of the process, SLM is capable of producing parts with a high geometrical complexity and almost no geometric constrictions. Thanks to the advantages of SLM [1], it is providing an ideal platform for producing Ti components and it has been increasingly employed to produce Ti and its alloys [1, 30-43]. It has been reported [31-37] that SLM can produce titanium alloys with comparable or even better mechanical properties compared to their counterparts processed by conventional production techniques. As such, the advantages of SLM process have potential to explore the application of SLM-produced alloys in such as biomedical, electronic and aeronautical industries. Among all the studied SLM-manufactured titanium alloys, Ti-6Al-4V alloy is the most frequently investigated thanks to its matured applications and the feedstock availability of powder suitable for SLM [1]. Considerable endeavours have been made to investigate the microstructural evolution of Ti-6Al-4V in the process of SLM with the aim to achieve utmost high density of the SLM-produced parts [36, 37, 40-42]. Microstructural characterizations indicate that the SLM-produced Ti-6Al-4V is dominated by fine acicular α′ martensite together with some prior β grains [36, 40, 44], which is distinct from the well-known α+β biphasic microstructure in traditionally processed Grade 5 alloy. SLM-produced Ti-6Al-4V is reported to commonly show improved mechanical properties compared to the ones processed by conventional techniques, which is mainly ascribed to the fine microstructure resulting from rapid solidification in the process of SLM [1]. So far, the most majority studies on the SLM-produced titanium alloys are focusing on their densification, microstructure and mechanical properties. In view of the high potential applications of SLM-produced Ti alloys in some corrosive environments, such as

corrosive chemical solution systems, human body and marine environment, apart from its mechanical properties, the corrosion resistance of SLM-produced titanium alloys is another critical property in term of its application in such environments. Unfortunately, so far there are extremely rare studies on the corrosion behaviour of SLM-produced samples. However, according to our previous study [44], the SLM-produced Ti-6Al-4V alloy possesses a slightly inferior corrosion resistance in comparison with the Grade 5 alloy in a 3.5 wt.% NaCl solution. This is mainly ascribed to the dominant acicular α' martensite in the SLM-produced Ti-6Al-4V alloy that is unfavourable to corrosion resistance. It is known that the mechanical properties of SLM-produced samples could be enhanced via tuning their microstructure by means of adjusting the scan strategies and build orientations in the process of SLM [40, 43]. It is interestingly to note that different scan strategies in SLM generally result in distinctions in the microstructure and mechanical properties of the SLM-produced Ti-6Al-4V. The SLM-produced Ti alloys on different sample planes show different microstructural characteristics thereby the mechanical properties due to some typical scan strategies. It is believed that the electrochemical corrosion resistance of the SLM-produced alloys may differ from the sample planes (i.e. the build plane and the build direction plane) due to their microstructural difference. Therefore, considering that the SLM-produced Ti alloys are in service in some environments, it is highly significant to further investigate the corrosion resistance of SLM-produced samples on different sample planes with different microstructure. This will give insight into the corrosion performance of SLM-produced samples and offering techniques to improve the anisotropy in corrosion resistance.

As such, the main objective of this work is to investigate the corrosion resistance property on different sample planes (i.e. XY-plane, the build plane; XZ-plane, the build direction plane) of the

SLM-produced Ti-6Al-4V alloy in 3.5 wt.% NaCl and 1 M HCl solution, and to distinguish the difference in corrosion resistance for different planes of the SLM-produced Ti-6Al-4V alloy. Electrochemical measurements including potentiodynamic polarization and electrochemical impedance spectroscopy (EIS) tests were carried out to study the corrosion behaviour of SLM-produced Ti-6Al-4V alloy. The mechanism for the corrosion resistance of SLM-produced samples on different planes was correlated to their microstructural characteristics. All discussion was based on the data obtained from electrochemical measurements in order to shed light on the corrosion resistance for different planes of SLM-produced Ti-6Al-4V alloy.

2. Experimental

2.1. Sample and solution preparation

The Ti-6Al-4V alloy cubic samples with size of 10 mm × 10 mm × 10 mm were manufactured by SLM in a MTT SLM 250 HL machine containing a 400 W Yb:YAG fiber laser with an 80 μm spot size. The SLM-produced samples were manufactured using a laser power (at the part bed) of 200 W (λ=1.06 μm) and laser scan speeds of 1250 mm/s. Both the hatch spacing (distance between scan lines) and the layer thickness were 100 μm. The layers were scanned using a continuous laser mode according to a zigzag pattern, which was alternated by 90° between each successive layer, as shown in Fig. 1(a). The density of the SLM-produced Ti-6Al-4V samples measured by using the Archimedes method confirmed that the SLM-produced Ti-6Al-4V samples had a relative density of greater than 99%. In addition, the chemical compositions for the SLM-produced Ti-6Al-4V alloy in wt.% were 0.01 C, 0.002 H, 0.14 O, 0.02 N, 0.22 Fe, 6.25 Ti, 4.04 V and Ti balance.

In order to minimize the effect of the potential surface defects on the corrosion resistance property of the SLM-produced samples, the SLM-produced Ti-6Al-4V cubic samples were halved along the build plane (XY-plane) or build direction (XZ-plane) into two parts with size of 10 mm × 10 mm × 5 mm for investigation. Fig. 1(b) schematically presents the three-dimensional diagram of SLM-produced Ti-6Al-4V alloy (with cube size of 10 mm × 10 mm × 10 mm) and two different cutting planes used in this work. As such, the samples with XZ-plane and XY-plane were obtained for the experiments in this work. Afterward, all alloy samples were mounted in a plastic tube and sealed with epoxy resin. The XZ-plane and XY-plane surfaces were polished with SiC paper down to 2000 grit, cleaned with double-distilled water, ultrasonically cleaned in ethanol, and dried in air. The prepared samples were used for immersion test, microstructure studies and as working electrodes for electrochemical experiments.

As for the immersion test, the samples were weighted before the test, and then immersed in 1 M HCl solution at room temperature (25 °C), the same test condition with electrochemical experiments. In addition, considering that the epoxy resin could absorb the water in HCl solution, a same-size epoxy resin was also prepared and immersed in the HCl solution as blank sample. After a 15-days immersion, all the samples were taken out, rinsed with double-distilled water, removed corrosion products, ultrasonically cleaned in ethanol, and dried in air, finally weighted for calculating weight loss.

With regard to the microstructural characterization of the alloys studied, a Kroll's solution was prepared as etchant solution [44]. The above-mentioned solutions were prepared with analytical grade reagents and double-distilled water.

2.2 Electrochemical measurements

Electrochemical measurements including open circuit potential (OCP), potentiodynamic polarization and electrochemical impedance spectroscopy (EIS) were conducted using a Solartron SI1280B electrochemical station in a conventional three-electrode cell. In the electrochemical measurements, a platinum sheet was used as counter electrode, a saturated calomel electrode (SCE) acted as the reference electrode, and the surface of the samples with an area of 1.0 cm^2 served as the working electrode. Prior to polarization and EIS tests, the samples were kept in the solution for enough time to attain a stable OCP. The potentiodynamic polarization curves were performed from potential range of –0.5 to +2.5 V versus OCP at a sweep rate of 0.1667 mV/s. Electrochemical impedance spectroscopy was acquired at the OCP potentiostatically. The frequency range for EIS was from 100 kHz to 10 mHz with an amplitude of 10 mV. All reported potentials in this work were relative to SCE. All the electrochemical measurements were carried out in 3.5 wt.% NaCl or 1 M HCl solution at room temperature (25 ± 1 ºC). NaCl solution was employed to simulate the system containing Cl^-, while the use of HCl was to simulate the hasher solution with low pH. The electrochemical tests were performed at least three times for data reproducibility.

2.3. Residual stress tests and microstructural analysis

The residual stress tests have been carried out through XRD using a D8 Discover (Bruker, Germany). The high-index crystal face, $(103)_{\alpha\text{-Ti}}$ of Ti-6Al-4V alloy, was chosen to calculate the residual stress. It is known that the interplanar spacing of high-index crystal face is relatively small, which can lead us to the accurate residual stress. The four angles from 0 to 45° were chosen

to test for getting residual stress, as known as side-incline method.

The phase constituents of SLM-produced Ti-6Al-4V samples on the XY-plane (i.e the build plane) and XZ-plane (i.e. the build direction plane) were identified by X-ray diffraction (XRD) using a Bruker D8Advance X-ray diffractometer with Cu Kα radiation at room temperature. All XRD patterns were recorded with 2θ range between 30º and 80º. The Jade 5.0 was employed to calculate the contents of the different phases in the SLM-produced Ti-6Al-4V alloy. The microstructural characteristics of the XY-plane and XZ-plane of the SLM-produced Ti-6Al-4V alloy samples were examined by an Olympus GX51 optical microscope (OM). The surface morphology of the SLM-produced alloys was characterized using scanning electron microscopy (SU1500, Japan).

3. Results

3.1. Microstructural studies

Fig. 2 presents the XRD patterns for the XY- and XZ-planes of the SLM-produced Ti-6Al-4V. As seen from Fig. 2, the SLM-produced Ti-6Al-4V alloy is apparently dominated by α′-Ti phase along with only small amount of β-Ti phase (evident by very weak β-Ti peaks). Vrancken [36] and Amaya-Vazquez [9] pointed out that the β-Ti phase in Ti-6Al-4V alloy is difficult to detect, or is always minority or absent. The peak near 2θ = 39.5° is normally assigned to β-Ti phase [45, 46] while according to some studies [47, 48], the peak near 2θ = 72° could be β-Ti or α-Ti phase. Although both XY-plane and XZ-plane of the SLM-produced Ti-6Al-4V consist of the same main phases, the several peaks of the main phases in the XY-plane and XZ-plane exhibit different corresponding intensities. This suggests different contents of the main phases in the XY-plane and

XZ-plane. According to the calculation of XRD patterns by means of Jade software, the volume fraction of each constituting phase estimated from the XRD patterns [49, 50] for the SLM-produced Ti-6Al-4V alloy on XY- and XZ-planes is summarized in Table 1. It is worth noting that the peaks of α′-Ti for SLM-produced alloy are located at the same 2θ with the peaks of α-Ti phase [51]. Besides, further optical microstructural observations confirm that the phases in the SLM-produced Ti-6Al-4V alloy are α′-Ti.

Fig. 3 displays the optical micrographs for XY- and XZ- planes of SLM-produced Ti-6Al-4V alloy. For the SLM-produced Ti-6Al-4V on XZ plane, as seen in Fig. 3(a), the build layer boundaries are remarkable, which are common and results from the layer-wise features of SLM technology [32]. More detailed analysis on the microstructure of XZ-plane has been discussed in our previous work [44]. In overall, both XZ-plane and XY-plane for the SLM-produced Ti-6Al-4V alloy display a predominantly large amount of acicular α′ martensite, which are evident by the most majority of areas in the optical micrographs in Fig. 3. Some defects such as several pores are also presented in the microstructure on both XY plane and XZ plane. It is proposed that the pores are liable to elongated along the scan direction and located at certain layers. The accumulation in powder denudation and the surface roughness across the layers considered as the main cause to the formation of pores [40]. Unlike the prior columnar β grains in XZ-plane (Fig. 3(a)), the prior β grains in XY-plane (Fig. 3(b)) are in a square shape, which is closely related to the scan strategy adopted in the process of SLM as shown in Fig. 1(a). According to Ref. [40], the presence of prior β grains is mainly attributed to the absence of nucleation barrier in solidification in the process of SLM. The occurrence of acicular α′ martensite in SLM-produced Ti-6Al-4V rather than the equilibrium α phase in Grade 5 is ascribed to: (i) the remarkably higher cooling rate (10^3-10^8 ºC/s)

in the process of SLM in comparison with the critical cooling rate (about 410 K/s) for forming α′ via martensitic transformation from β in Ti-6Al-4V, and/or (ii) a high thermal gradient (10^4-10^5 ºC/cm) along the build direction in tiny melt pool [1].

3.2. Electrochemical studies

Fig. 4 presents the variation of OCP with time for the XY- and XZ- planes of the SLM-produced Ti-6Al-4V alloy immersed in 1 M HCl. The open circuit potential of both planes keeps shifting positively during immersion in HCl. This is mainly related to the formation of the passive film on the alloy surface. The generation of the film makes the anodic process control the electrode process, leading to the positive shifting of the OCP. After immersion for 45 h, it has difficulty for XY- and XZ- planes to obtain a perfectly stable potential. However, the potential increases slightly at a potential change rate of ~1.5 mV/h. Such a little potential change at 1.5 mV/h gives no significant influence on the subsequent EIS tests. The relatively stable OCPs for the XY-plane (i.e. –149.7 ± 8.3 mV) and XZ-plane (i.e. –175.0 ± 5.9 mV) of the SLM-produced Ti-6Al-4V are very close, but the final OCP of XY-plane is slightly higher than that of XZ-plane. In our previous study [44], the OCP value for SLM-produced Ti-6Al-4V maintained at approximately 90 mV after 60h immersion in a 3.5 wt. % NaCl solution, which is much nobler than that of the SLM-produced Ti-6Al-4V in HCl solution.

Fig. 5 shows the potentiodynamic polarization curves of SLM-produced Ti-6Al-4V alloy on both XY-plane and XZ-plane in 3.5 wt.% NaCl solution and 1 wt.% HCl solution. Before polarization tests, it took enough time to achieve a relatively stable open circuit potential (OCP). The SLM-produced Ti-6Al-4V on XY-plane and XZ-plane display evident passivated behaviour in

the potential range between 200 mV and 1500 mV in 1 M HCl solution and from 200 mV to 1200 mV in 3.5 wt.% NaCl solution. This means that a passive film has formed in the mentioned potential range in corrosive solutions, which works as a protective film to inhibit the corrosion of titanium alloys with regards to the service in corresponding solution media. Note that, the SLM-produced Ti-6Al-4V alloy displays a broader potential range (ΔE_2) for the passive film in 1 M HCl solution in comparison with that (ΔE_1) in 3.5 wt.% NaCl solution. As can be seen in Fig. 4, i_p stands for the passivation current for the film formed on the alloy surface, normally the lower i_p means the easy passivation of the alloys and i_p represents the total current density of the metal dissolution and quick deposition of the corrosion products. Thus the lower i_p, easy passivation of Ti-6Al-4V alloy normally exhibits the better corrosion resistance in corresponding solution systems. For the corrosion behaviour of SLM-produced Ti-6Al-4V in 3.5 wt.% NaCl solution, the i_p for both XY-plane and XZ-plane are very close ($i_{p,XY} = i_{p,XZ} = 0.76 \pm 0.013$ $\mu A \cdot cm^{-2}$). More details on the value of the i_p in NaCl solution could also be referred to our previous report [44].

In the case of corrosion behaviour of SLM-produced Ti-6Al-4V in HCl solution, $i_{P,XY}$ and $i_{P,XZ}$ refer to the passivation current of XY- and XZ-planes in 1 M HCl solution respectively. The value of the passivation current for the XZ-plane of SLM-produced Ti-6Al-4V alloy, $i_{P,XZ}$, is 2.83 $\pm$ 0.04 $\mu A \cdot cm^{-2}$. The $i_{P,XY}$ is 2.50 $\pm$ 0.02 $\mu A \cdot cm^{-2}$, which is slightly lower than the $i_{P,XZ}$. In general, a lower passivation current i_p indicates an easy passivation of the film or a slow dissolution of alloy. As such, the comparison between the above mentioned values of passivation current (i_p) for the SLM-produced Ti-6Al-4V on the XY-plane and XZ-plane suggests that the XY-plane of SLM-produced Ti-6Al-4V alloy has a slightly better corrosion resistance than the XZ-plane in 1 M HCl solution. In other words, there exists anisotropy in corrosion resistance of different planes

(such as the build plane and the build direction plane) of the SLM-produced Ti-6Al-4V in 1 M HCl solution in spite of very slight difference in NaCl solution.

The EIS measurements were carried out to investigate the surface condition immersed in corresponding solutions. Fig. 6 shows the Nyquist and Bode plots of the XY- and XZ- planes of the SLM-produced Ti-6Al-4V alloy in 1 M HCl solution. The inset figures of Nyquist plots for XY- and XZ- planes of the SLM-produced Ti-6Al-4V alloy in 3.5 wt.% NaCl solution and equivalent circuit for fitting the EIS data are shown in Fig. 6(a). In the equivalent circuit, R_s is the solution resistance, the R_{ct} and C_{dl} correspond to the charge transfer resistance and double layer capacitance, respectively. The R_f and CPE_1 refer to the film resistance and film capacitance respectively. As seen in Fig. 6(a), the Nyquist plots exhibit only a big capacitive loop for each sample, but the Bode plots (Fig. 6 (b)) show a plateau in a range of a wide frequency (from high frequency to low frequency). As such, an equivalent circuit with two time-constants was used to fit the EIS data. Table 2 summarizes the fitted results of the EIS measurements. As for the SLM-produced Ti-6Al-4V alloy in 3.5 wt.% NaCl solution, the fitted results of R_f (Table 2) have very close values for XY-plane and XZ-plane; the same as for the R_{ct} values. This suggests that the XY- and XZ-planes exhibit no obvious distinction in corrosion resistance in 3.5 wt.% NaCl solution, which is in well agreement with the results in polarization tests. In contrast, for the SLM-produced Ti-6Al-4V alloy in 1 M HCl solution, i.e. a harsher solution system, the R_f value of XY-plane is several times that of XZ-plane. This reveals the fact that the passive film formed on the XY-plane of SLM-produced Ti-6Al-4V possesses a better protective property than the XZ-plane. The result of R_{ct} also supports the conclusion from the analysis of R_f. All these findings suggest that the distinction in corrosion resistance between XY- and XZ-plane is more evident in a

harsher solution, regarding the application of the SLM Ti-6Al-4V in some typical solution environments.

According to the immersion tests, the weight loss for XY-plane was 0.7 (±0.05) mg/cm^2, while 0.9 (±0.1) mg/cm^2 for XZ-plane which is a bit higher than that of XY-plane. As such, the results of weight loss can support the electrochemical test. At present, there are also some studies performed immersion tests to study the corrosion behavior of Ti-based alloys in some solution systems with a high Cl^- concentration at a higher temperature [52-54]. In addition, the SEM images of the XZ- and XY- planes of the SLM-produced Ti-6Al-4V sample after electrochemical corrosion (polarization) were shown in Fig. 7. According to the SEM images, some pores are observed in the microstructure of the SLM-produced Ti-6Al-4V alloy (include XY- and XZ-planes). These pores pre-existing in the microstructure re-appear after electrochemical corrosion in the microstructure. Furthermore, some more pits are generated in the microstructure of the XZ-plane of the SLM-produced alloy than that in the XY-plane, suggesting that the passive film formed on the XZ-plane exhibits an inferior stability and protective ability than that on the XY-plane.

4. Discussion

According to the residual stress tests, the value of residual stress for XY-plane was 114.9 MPa, while it was 128.7 MPa for XZ-plane which is a bit higher than that for XY-plane. Yet, it seems that the values for two different planes were extremely close. As for Ti-6Al-4V alloy, the residual stress value in this range gives no rise to the corrosion resistance. In other words, the corrosion resistance for different planes of SLM-processed alloy has no evident relation with the

residual stress.

The results of the electrochemical experiments were used to study the corrosion resistance of the SLM-produced Ti-6Al-4V alloy on XY-plane and XZ-plane. According to the potentiodynamic curves (Fig. 5), a passive film is formed on the alloy during the anodic potential range, which suggests that the formation of the film inhibits the corrosion of alloy. The passivation currents for the alloys on XZ-plane in 1 M HCl solution is slightly greater than that on XY-plane, i.e. $i_{P,XZ}$ (2.834 ± 0.041 $\mu A \cdot cm^{-2}$) > $i_{P,XY}$ (2.498 ± 0.023 $\mu A \cdot cm^{-2}$). In this work, it is believed that the XY-plane of the SLM-produced Ti-6Al-4V shows a better corrosion resistance in comparison with the XZ-plane in terms of the values of both the film resistance (R_f) and the passivation current (i_P). Herein, comparing with the SLM Ti-6Al-4V alloy in 3.5 wt.% NaCl solution, the potential range of the passive film formed on SLM alloy in 1 M HCl solution was broader ($\Delta E_2 > \Delta E_1$). While the passivation current ($i_{P,XY}$ and $i_{P,XZ}$) of film formed on SLM-produced Ti-6Al-4V in 1 M HCl solution are higher than the corresponding ones ($i_{P,XY} = i_{P,XZ}$) in 3.5 wt.% NaCl solution. This suggests that the SLM-produced Ti-6Al-4V exhibits a higher corrosion rate in 1 M HCl solution. Simultaneously, the difference in corrosion resistance between XY- and XZ-planes in 1 M HCl solution is more evident than in 3.5wt.% NaCl solution. As seen in Fig. 7, after electrochemical measurements (beyond passive potential) for the XY- and XZ- planes of the SLM-produced alloy, apart from the former pores, more pits have developed in the XZ-plane than in XY-plane. On the other hand, it reveals that the passive film formed on the XZ-plane is not resistant and stable enough against the electrochemical corrosion, which is in good agreement with the R_f results for the XZ- and XY-planes in EIS tests.

It is noted that the microstructure of a material has a vital impact on its corrosion resistance.

Unlike the typical microstructure of commercial Grade 5 alloy [44], the acicular α′ martensitic phase dominates the microstructure of the SLM-produced Ti-6Al-4V alloy. Although the microstructure of the SLM-produced Ti-6Al-4V alloy (and other materials as well) was extensively investigated [36, 37, 40-42], the quantitative percentage of the corresponding phases in the microstructure of SLM-produced alloy has rarely been reported. Estimated from the XRD patterns (Fig. 1), the amount of α′-Ti and β phase in the SLM-produced Ti-6Al-4V alloy are 88.1% and 11.9% respectively in the XY-plane and 95.0% and 5.0% respectively in the XZ-plane. As discussed in previous work [44], the acicular α′ martensitic phase is in "high energy state" and metastable with regard to corrosion. As for different planes in SLM-produced alloy, the XZ-plane with more amount of α′-Ti phase in the microstructure results in an inferior corrosion resistance than the XY-plane. Simultaneously, the more content of β-Ti phase in XY-plane also enhances the corrosion resistance. More discussion on the corresponding content can be referred to our former study [44]. Therefore, the difference in the volume fraction of α′ and β phases results in the distinction in electrochemical activity or corrosion resistance of SLM-produced Ti-6Al-4V on different sample planes. In addition, analysing the R_f for the different planes of the SLM-produced Ti-6Al-4V (Table 2) also suggests that the XY-plane possesses a better corrosion resistance than the XZ-plane of the SLM-produced alloy, which is well consistent with the results obtain from polarization curves. Furthermore, the charge transfer resistance (R_{ct}) can also support the corresponding conclusion. All these results are well consistent with the polarization tests (Fig. 5) and the discussion based on the microstructure (Figs. 2 and 3). Thus, the different planes of SLM-produced Ti-6Al-4V usually display different microstructural characteristics (such as phase constituents and/or phase fractions) owing to the scan strategies used, resulting in the distinct

corrosion resistance of the different planes of the SLM-produced alloys. As for these reasons, it is of importance to select with caution the working surface of the SLM-produced Ti-6Al-4V alloy for better corrosion resistance with regards to its application in some harsh environments, as well as solution system containing strong corrosive ions.

5. Conclusion

In 1 M HCl solution, the XY-plane shows a better corrosion resistance in comparison with the XZ-plane of the SLM-produced Ti-6Al-4V alloy, even if the very slight difference between XY- and XZ-planes in 3.5 wt.% NaCl solution. The microstructure of the SLM-produced Ti-6Al-4V alloy is overwhelmingly dominated by acicular α′ martensitic phase along with trace β-Ti phase. The XZ-plane of the SLM-produced Ti-6Al-4V alloy is composed of more α′-Ti and less β-Ti phase than XY-plane, which lead to the inferior corrosion resistance of XZ-plane. Thus the difference in the corrosion resistance property is attributed to the distinction in amount of the α′ phase and β-Ti phase in microstructure.

Acknowledgements

The research was supported under the Australian Research Council's Projects funding scheme (DP110101653). This work was also supported by Science and Technology Commission of Shanghai Municipality (No: 14DZ2261000). The authors gratefully acknowledge the technical support of metallographic examination from Lei Yang.

References

[1] L.C. Zhang, H. Attar, Selective laser melting of titanium alloys and titanium matrix composites

for biomedical applications: a review, Adv. Eng. Mater. 18 (2016) 463-475.

[2] J.R. Chen, W.T. Tsai, In situ corrosion monitoring of Ti-6Al-4V alloy in H_2SO_4/HCl mixed solution using electrochemical AFM, Electrochim. Acta 56 (2011) 1746-1751.

[3] S. Tamilselvi, V. Raman, N. Rajendran, Corrosion behaviour of Ti-6Al-7Nb and Ti-6Al-4V ELI alloys in the simulated body fluid solution by electrochemical impedance spectroscopy, Electrochim. Acta 52 (2006) 839-846.

[4] B. Gunawarman, M. Niinomi, T.A. Wallace, J. Takeda, H. Toda, Mechanical properties of Ti-4.5Al-3V-2Mo-2Fe and possibility for healthcare applications, Mater. Sci. Eng. C 25 (2005) 296-303.

[5] G.B. Cho, K.W. Kim, H.J. Ahn, K.K. Cho. T.H. Nam, Applications of Ti-Ni alloys for secondary batteries, J. Alloys Comp. 449 (2008) 317-321.

[6] S. Krischok, C. Blank, M. Engel, R. Gutt, G. Ecke, J. Schawohl, L. Spie, F. Schrempel, G. Hildebrand, K. Liefeith, Influence of ion implantation on titanium surfaces for medical applications, Surf. Sci. 601 (2007) 3856-3860.

[7] S.E. Haghighi, H.B. Lu, G.Y. Jian, G.H. Cao, D. Habibi, L.C. Zhang, Effect of α″ martensite on the microstructure and mechanical properties of beta-type Ti-Fe-Ta Alloys, Mater. Design 76 (2015) 47-54.

[8] S. Ehtemam-Haghighi, Y. Liu, G. Cao, L.C. Zhang, Influence of Nb on the β→α" martensitic phase transformation and properties of the newly designed Ti-Fe-Nb alloys, Mater. Sci. Eng. C 60 (2016) 503-510.

[9] M.R. Amaya-Vazquez, J.M. Sanches-Amaya, Z. Boukha, F.J. Botana, Microstructure, microhardness and corrosion resistance of remelted TiG2 and Ti6Al4V by a high power diode

layer, Corros. Sci. 56 (2012) 36-48.

[10] V.A. Alves, R.Q. Reis, I.C.B. Santos, D.G. Souza, T. de F. Goncalves, M.A. Pereira-da-Silva, A. Rossi, L.A. da Silva, In situ impedance spectroscopy study of the electrochemical corrosion of Ti and Ti-6Al-4V in simulated body fluid at 25°C and 37°C, Corros. Sci. 51 (2009) 2473-2482.

[11] R.Sh. Razavi, M. Salehi, M. Ramazani, H.C. Man, Corrosion behaviour of laser gas nitride Ti-6Al-4V in HCl solution, Corros. Sci. 51 (2009) 2324-2329.

[12] C.E.B. Marino, S.R. Biaggio, R.C. Rocha-Filho, N. Bocchi, Voltammetric stability of anodic films on the Ti6Al4V alloy in chloride medium, Electrochim. Acta 51 (2006) 6580-6583.

[13] R. Gaddam, R. Pederson, M. Hörnqvist, M-L. Antti, Fatigue crack growth behaviour of forged Ti–6Al–4V in gaseous hydrogen, Corros. Sci. 78 (2014) 378-383.

[14] J.E.G. Gonzalez, J.C. Mirza-Rosca, Study of the corrosion behavior of titanium and some of its alloys for biomedical and dental implant applications, J. Electroanal. Chem. 471 (1999) 109-115.

[15] N. Ibris, J.C. Mirza-Rosca, EIS study of Ti and its alloys in biological media, J. Electroanal. Chem. 526 (2002) 53-62.

[16] E. Galvanetto, F.P. Galliano, A. Fossati, F. Borgioli, Corrosion resistance properties of plasma nitride Ti-6Al-4V alloy in hydrochloric acid solutions, Corros. Sci. 44 (2002) 1593-1606.

[17] F. El-Taib Heakal, A.A. Ghoneim, A.S. Mogoda, Kh. Award, Electrochemical behaviour of Ti-6Al-4V alloy and Ti in azide and halide solutions, Corros. Sci. 53 (2011) 2728-2737.

[18] N. Zaveri, M. Mahapatra, A. Deceuster, Y. Peng, L.J. Li, A.H. Zhou, Corrosion resistance of pulsed laser-treated Ti-6Al-4V implant in simulated biofluids, Electrochim. Acta 53 (2008) 5022-5032.

[19] G.E. Ryan, A.S. Pandit, D.P. Apatsidis, Porous titanium scaffolds fabricated using a rapid prototyping and powder metallurgy technique, Biomaterials 29 (2008) 3625-3635.

[20] C.Q. Ning, Y. Zhou, In vitro bioactivity of a biocomposite fabricated from HA and Ti powders by powder metallurgy method, Biomaterials 23 (2002) 2909-2915.

[21] P.J. Kwok, S.M. Oppenheimer, D.C. Dunand, Porous Titanium by Electro-chemical Dissolution of Steel Space-holders, Adv. Eng. Mater. 10 (2008) 820-825.

[22] S.A. Tsipas, E. Gordo, A. Jiménez-Morales, Oxidation and corrosion protection by halide treatment of powder metallurgy Ti and Ti6Al4V alloy, Corros. Sci. 88 (2014) 263-274.

[23] L. Benea, E. Mardare-Danaila, M. Mardare, J.P. Celis, Preparation of titanium oxide and hydroxyapatite on Ti–6Al–4V alloy surface and electrochemical behaviour in bio-simulated fluid solution, Corros. Sci. 80 (2014) 331-338.

[24] V.M.C.A. Oliveira, C. Aguiar, A.M. Vazquez, A. Robin, M.J.R. Barboza, Improving corrosion resistance of Ti–6Al–4V alloy through plasma-assisted PVD deposited nitride coatings, Corros. Sci. 88 (2014) 317-327.

[25] W.B. Li, S.L. Zhu, C. Wang., M.H. Chen, M.L. Shen, F.H. Wang, SiO_2–Al_2O_3–glass composite coating on Ti–6Al–4V alloy: Oxidation and interfacial reaction behaviour, Corros. Sci. 74 (2013) 367-378.

[26] L. Benea, E. Danaila, P. Ponthiaux, Effect of titania anodic formation and hydroxyapatite electrodeposition on electrochemical behaviour of Ti–6Al–4V alloy under fretting conditions for biomedical applications, Corros. Sci. 91 (2015) 262-271.

[27] Anawati, H. Tanigawa, H. Asoh, T. Ohno, M. Kubota, S. Ono, Electrochemical corrosion and bioactivity of titanium–hydroxyapatite composites prepared by spark plasma sintering, Corros. Sci.

70 (2013) 212-220.

[28] Y.J. Chen, B. Feng, Y.P. Zhu, J. Weng, J.X. Wang, X. Lu, Fabrication of porous titanium implants with biomechanical compatibility, Mater. Lett. 63 (2009) 2659-2661.

[29] I.M. Pohrelyuk, V.M. Fedirko, O.V. Tkachuk, R.V. Proskrnyak, corrosion resistance of Ti-6Al-4V alloy with nitride coatings in Ringer's solution, Corros. Sci. 66 (2013) 392-398.

[30] J.P. Kruth, G. Levy, F. Klocke, T.H.C. Childs, Consolidation phenomena in laser and powder-bed based layered manufacturing, CIRP Ann. – Manuf. Technol. 56 (2007) 730-759.

[31] L. Mullen, R.C. Stamp, W.K. Brooks, E. Jones, C.J. Sutcliffe, Selective laser melting: a regular unit cell approach for the manufacture of porous, titanium, bone in-growth constructs, suitable for orthopaedic applications, J. Biomed. Mater. Res. B 89B (2009) 325-334.

[32] L.C. Zhang, D. Klemm, J. Eckert, Y.L. Hao, T.B. Sercombe, Manufacture by selective laser melting and mechanical behavior of a biomedical Ti-24Nb-4Zr-8Sn alloy, Scripta Mater. 65 (2011) 21-24.

[33] H. Attar, K.G. Prashanth, A.K. Chaubey, M. Calin, L.C. Zhang, S. Scudino, J. Eckert, Comparison of wear properties of commercially pure titanium prepared by selective laser melting and casting processes, Mater. Lett. 142 (2015) 38-41.

[34] H. Attar, M. Bönisch, M. Calin, L.C. Zhang, S. Scudino, J. Eckert, Selective laser melting of in-situ titanium-titanium boride composites: Processing, microstructure and mechanical properties, Acta Mater. 76 (2014) 13-22.

[35] H. Attar, M. Calin, L.C. Zhang, S. Scudino, J. Eckert, Manufacture by selective laser melting and mechanical behavior of commercially pure titanium, Mater. Sci. Eng. A 593 (2014) 170-177.

[36] B. Vrancken, L. Thijs, J.P. Kruth, J.V. Humbeeck, Heat treatment of Ti6Al4V produced by

Selective Laser Melting: Microstructure and mechanical properties, J. Alloys Comp. 54 (2012) 177-185.

[37] D. D. Gu, Y. C. Hagedorn, W. Meiners, G. Meng, R. J. S. Batista, K. Wissenbach, R. Poprawe, Densification behavior, microstructure evolution, and wear performance of selective laser melting processed commercially pure titanium, Acta Mater. 60 (2012) 3849-3860.

[38] Y.J. Liu, X.P. Li, L.C. Zhang, T.B. Sercombe, Processing and properties of topologically optimised biomedical Ti-24Nb-4Zr-8Sn scaffolds manufactured by selective laser melting, Mater. Sci. Eng. A 642 (2015) 268-278.

[39] Y.J. Liu, S.J. Li, H.L. Wang, W.T. Hou, Y.L. Hao, R. Yang, T.B. Sercombe, L.C. Zhang, Microstructure, defects and mechanical behavior of beta-type titanium porous structures manufactured by electron beam melting and selective laser melting. Acta Materialia 113 (2016) 56-67.

[40] L. Thijs, F. Verhaeghe, T. Craeghs, J.V. Humbeeck, J.P. Kruth, A study of the microstructural evolution during selective laser melting of Ti-6Al-4V, Acta Mater. 58 (2010) 3303-3312.

[41] I. Yadroitsev, P. Krakhmalev, I. Yadroitsava, Selective laser melting of Ti6Al4V alloy for biomedical applications: Temperature monitoring and microstructural evolution, J. Alloys Comp. 583 (2014) 404-409.

[42] E. Sallica-Leva, A.L. Jardini, J.B. Fogagnolo, Microstructure and mechanical behavior of porous Ti-6Al-4V obtained by selective laser melting, J. Mech. Behav. Biomed. Mater. 26 (2013) 98-108.

[43] R. Wauthle, B. Vrancken, B. Beynaerts, K. Jorissen, J. Schrooten, J.P. Kruth, J.V. Humbeeck, Effects of build orientation and heat treatment on the microstructure and mechanical properties of

selective laser melted Ti6Al4V lattice structures, Add. Manuf. 5 (2015) 77-84.

[44] N. Dai, L.C. Zhang, J. Zhang, Q. Chen, M. Wu, Corrosion Behaviour of Selective Laser Melted Ti-6Al-4V Alloy in NaCl Solution, Corros. Sci. 102 (2016) 484-489.

[45] L. Facchini, A. Molinari, S. Hoges, K. Wissenbach, Ductility of a Ti-6Al-4V alloy produced by selective laser melting of prealloyed powders, J. Rapid. Prototyping 16 (2010) 450–459.

[46] M.T. Jovanovic, C. Tadic, S. Zec, Z. Miskovic, I. Bobic, The effect of annealing temperatures and cooling rates on microstructures and mechanical properties of investment cast Ti6Al4V alloy, Mater. Des. 27 (2006) 192–199.

[47] S.L. Sing, W.Y. Yeong, F.E. Wiria, Selective laser melting of titanium alloy with 50 wt% tantalum: Microstructure and mechanical properties, J. Alloys. Comp. 660 (2016) 461-470.

[48] S.M. Bhola, S. Kundu, R. Bhola, B. Mishra, S. Chatterjee, Electrochemical study of diffusion bonded joints between Micro-duplex stainless steel and Ti6Al4V alloy, J. Mater. Sci. Technol. 30 (2014) 163-171.

[49] L.C. Zhang, Z.Q. Shen, J. Xu, Glass formation in a (Ti, Zr, Hf)-(Cu, Ni, Ag)-Al high-order alloy system by mechanical alloying, J. Mater. Res. 18 (2003) 2141-2149.

[50] L.C. Zhang, J. Das, H.B. Lu, C. Duhamel, M. Calin, J. Eckert, High strength Ti-Fe-Sn ultrafine composites with large plasticity, Scripta Mater. 57 (2007) 101-104.

[51] R.W. Boyer, G.E.W. Collings, Materials properties handbook: titanium alloys, Material Park (OH): ASM International, 1994.

[52] M. Atapour, A.L. Pilchak , G.S. Frankel, J.C. Williams, Corrosion behavior of β titanium alloys for biomedical applications, Mater. Sci. Eng. C 31 (2011) 885-891.

[53] M. Atapour, A.L. Pilchak, M. Shamanian, M.H. Fathi, Corrosion behavior of Ti–8Al–1Mo–

1V alloy compared to Ti–6Al–4V, Mater. Des. 32 (2011) 1692-1696.

[54] S. Karimi, T. Nickchi, A.M. Alfantazi, Long-term corrosion investigation of AISI 316L, Co–28Cr–6Mo, and Ti–6Al–4V alloys in simulated body solutions, Appl. Surf. Sci. 258 (2012) 6087-6096.

Figure captions:

Fig. 1. Schematic representation of (a) laser scan direction and angle between the successive layers in the process of SLM and (b) three-dimensional diagram of SLM-produced Ti-6Al-4V alloy cubic samples with size of 10 mm × 10 mm × 10 mm and two different studied planes.

Fig. 2. XRD patterns for the XY- and XZ-planes of the SLM-produced Ti-6Al-4V alloy.

Fig. 3. Optical microstructure of the (a) XZ-plane and (b) XY-plane of SLM-produced Ti-6Al-4V sample (build direction is normal to the paper). The insets show the magnified images corresponding to the each plane of the SLM-produced alloy.

Fig. 4. Variation of open circuit potential (OCP) with time for the XY- and XZ- planes of SLM-produced Ti-6Al-4V alloy immersed in 1 M HCl solution.

Fig. 5. Potentiodynamic curves for the XY- and XZ-planes of SLM-produced Ti-6Al-4V alloy in 3.5 wt.% NaCl solution and 1 M HCl solution (test three times for each sample).

Fig. 6. The EIS measurements for the XY- and XZ- planes of SLM-produced Ti-6Al-4V alloy in 1M HCl: (a) Nyquist plots, (b) Bode plots. The inset figures in (a) were Nyquist plots for XY- and XZ- planes of SLM-produced Ti-6Al-4V alloy in 3.5 wt.% NaCl solution and equivalent circuit used to impedance spectra analysis.

Fig. 7. SEM images of the (a) XZ-plane and (b) XY- planes of SLM-produced Ti-6Al-4V alloy after electrochemical corrosion.

Figures:

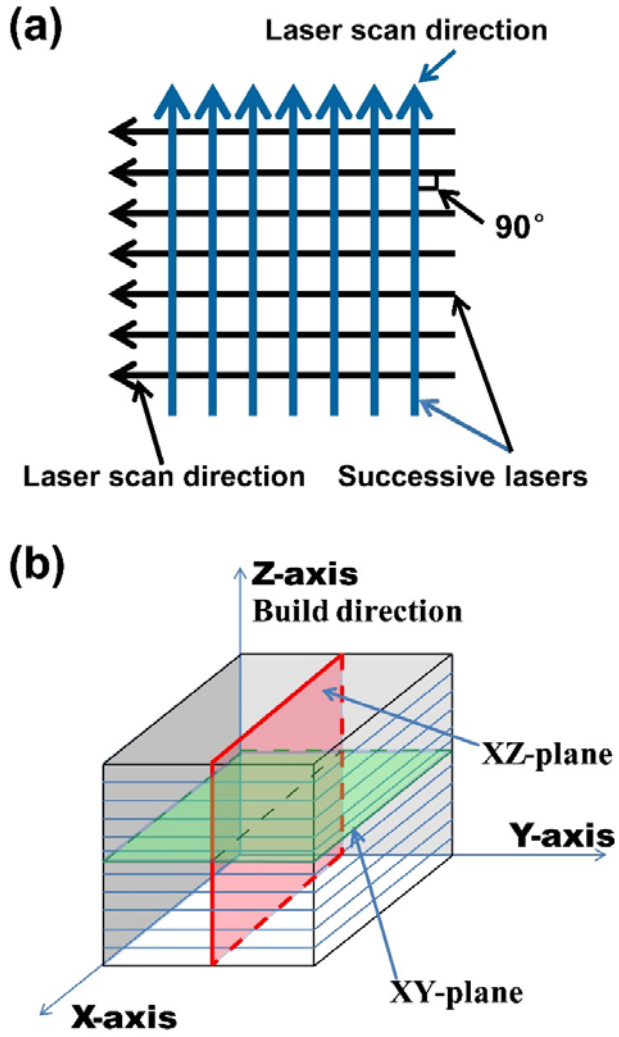

Fig. 1.

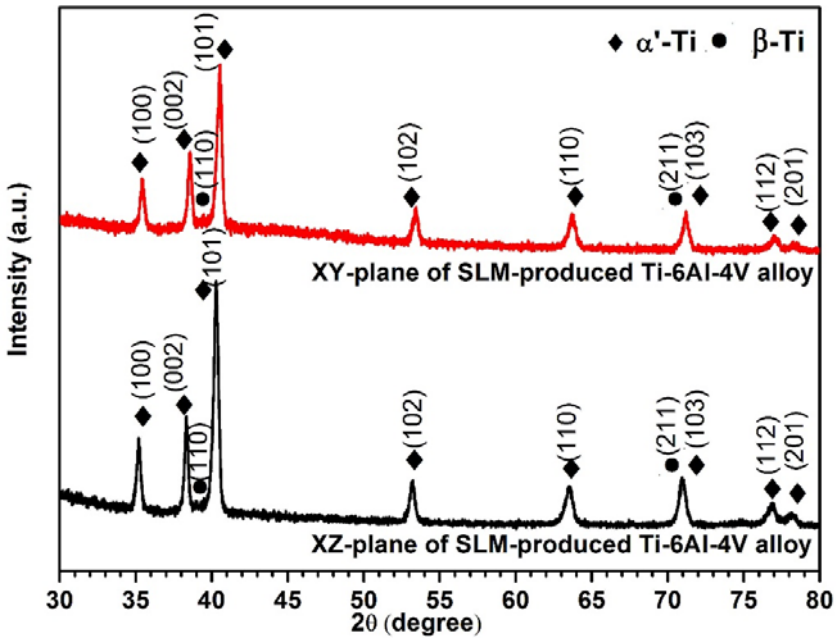

Fig. 2.

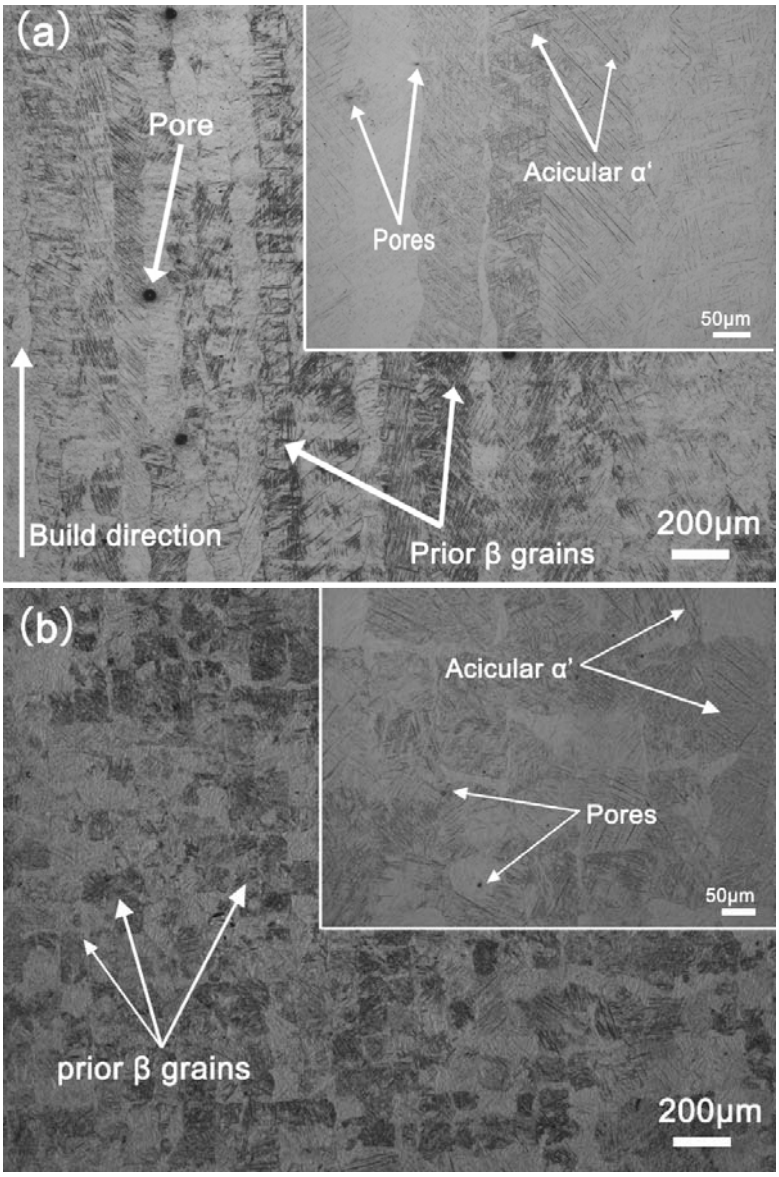

Fig. 3.

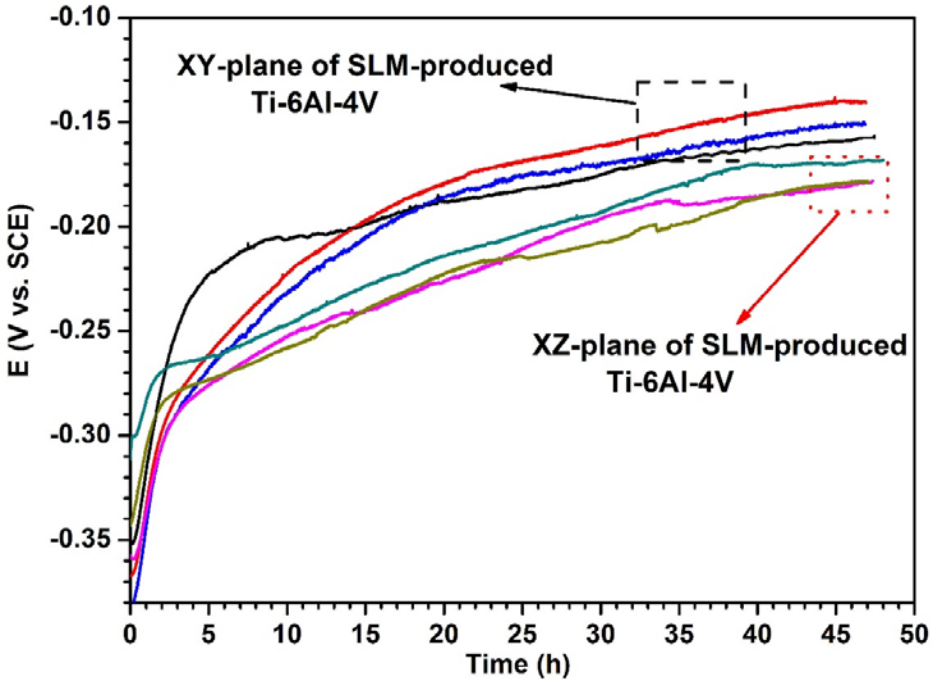

Fig. 4.

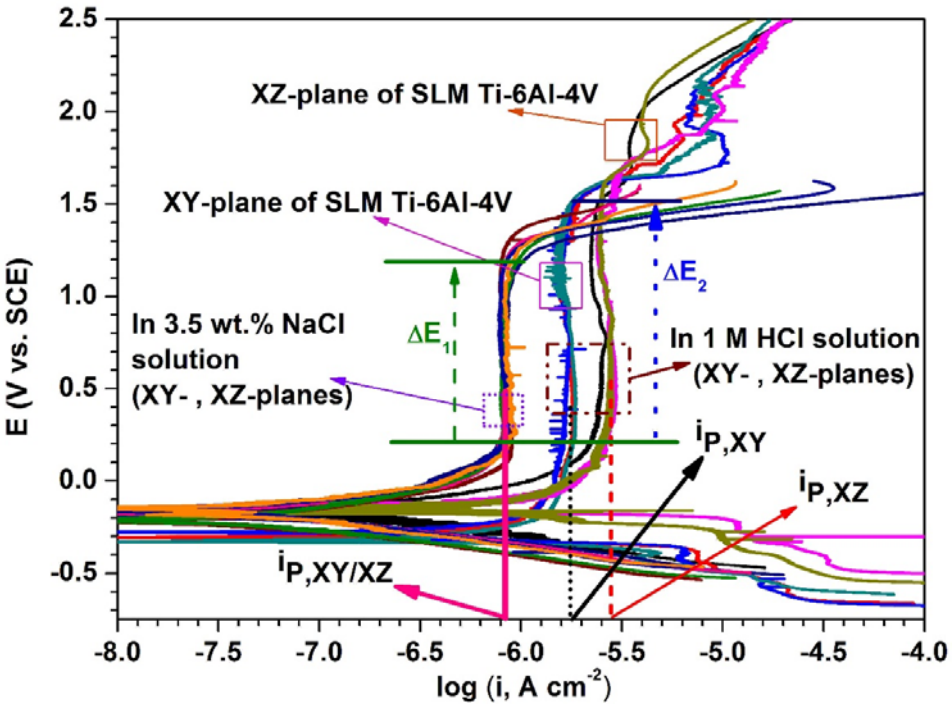

Fig. 5.

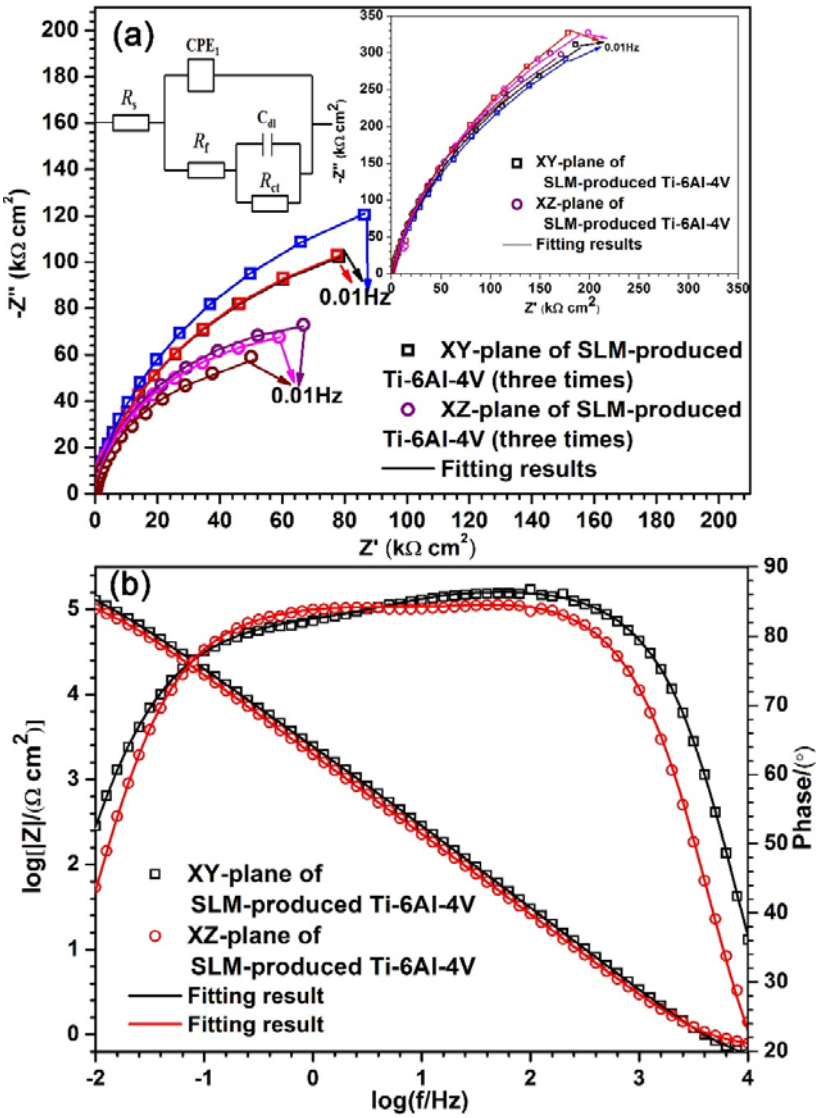

Fig. 6.

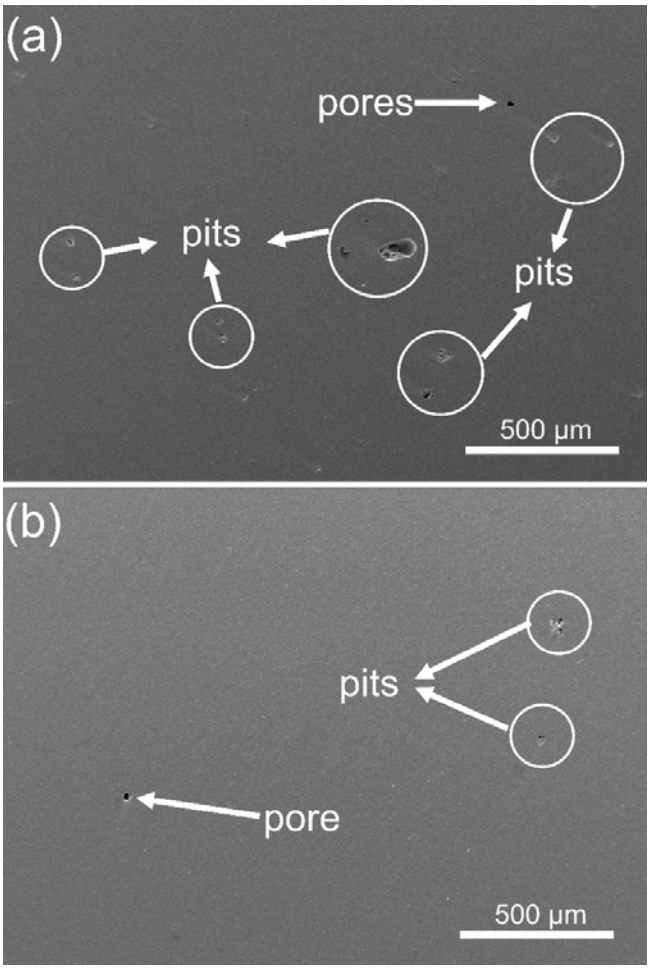

Fig. 7.

Tables:

Table 1 Phase constituents and their volume fraction (V_f) of XY- and XZ-planes of the SLM-produced Ti-6Al-4V alloy estimated from the XRD patterns.

Sample	Phase constituents	$V_{f,\alpha}$ *or* $V_{f,\alpha'}$	$V_{f,\beta}$
SLM-produced, XY-plane	$\alpha' + \beta$	88.1%	11.9%
SLM-produced,XZ-plane	$\alpha' + \beta$	95.0%	5.0%

Table 2 The fitting parameters of EIS measurements forthe XY- and XZ- planes of SLM-produced Ti-6Al-4V alloy in 1 M HCl and 3.5 wt.%NaCl solution. R_s: the solution resistance, R_f: the film resistance, R_{ct}: the charge transfer resistance, C_{dl}: the double layer capacitance, and CPE_1: the film capacitance respectively.

Solution	Sample	R_f ($k\Omega \cdot cm^2$)	CPE_1, Y_0 ($S \cdot Sec^n \cdot cm^{-2}$)	n_1	R_{ct} ($k\Omega \cdot cm^2$)	C_{dl} ($\mu F \cdot cm^{-2}$)
1 M HCl	SLM-produced, XY-plane	5.63	60.10	0.9697	293.30	39.40
	Error	0.62	0.32	0.0019	0.33	0.50
	SLM-produced, XZ-plane	1.67	94.22	0.9496	129.70	25.88
	Error	0.42	0.24	0.0087	0.23	0.49
3.5 wt.% NaCl	SLM-produced, XY-plane	26.84	26.58	0.9107	814.90	408.50
	Error	3.27	1.69	0.0029	17.47	36.51
	SLM-produced, XZ-plane	22.69	20.53	0.8974	798.30	404.20
	Error	3.00	1.07	0.0066	12.61	17.75